Journal of Chemical&Engineering Data

pubs.acs.org/jced
Article

Molecular Modeling of HFC Separation in Fluorinated Ionic Liquids: A SAFT-VR Mie Study

Published as part of Journal of Chemical & Engineering Data special issue "In Honor of Frederico W. Tavares".

Isaías Huenuvil-Pacheco, Andrés Mejía, and Fèlix Llovell*

Cite This: J. Chem. Eng. Data 2025, 70, 4939−4953

Read Online

ACCESS | Metrics & More | Article Recommendations | Supporting Information

ABSTRACT: Given the critical role of hydrofluorocarbons (HFCs) in the refrigeration industry, their recovery is crucial to promoting circular economy strategies and reducing greenhouse gas emissions. In this work, the SAFT-VR Mie equation of state is applied to describe the solubility of R32, R125, and R134a in ionic liquids (ILs) with varying degrees of fluorination, which are proposed as potential absorbents for gas separation. ILs are treated as associating species, with multiple sites accounting for charge delocalization. The model provides an excellent description of density and viscosity, the latter obtained through the Helmholtz scaling theory. In addition, the effect of polarity is explicitly accounted for in the HFCs. As a result, their solubility in ILs is quantitatively reproduced using a single, temperature-independent binary parameter, ensuring a strong predictive capability. Furthermore, the working capacity and competitive selectivity of the components in commercial R410A and R407F blends are predicted, revealing significant differences in performance depending on the solvent composition and fluorination level. Additional properties, such as regeneration enthalpy and viscosity, are also evaluated to identify the most promising ILs for refrigerant recovery. Overall, this study demonstrates the capability of SAFT-VR Mie as a robust molecular-based tool for solvent screening in sustainable HFC separation technologies.

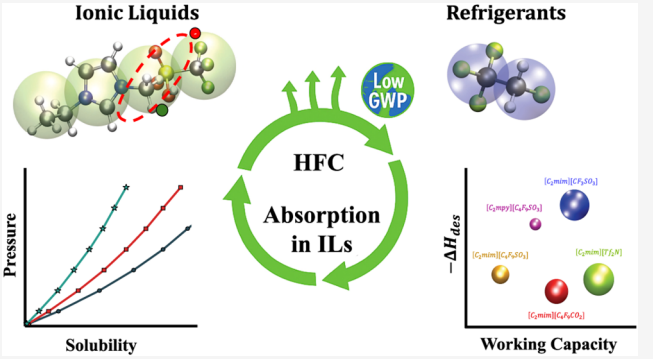

INTRODUCTION

The progressive reduction of ozone-depleting chlorofluorocarbons (CFCs) and hydrochlorofluorocarbons (HCFCs) has led to the widespread adoption of hydrofluorocarbons (HFCs) in refrigeration, air conditioning, and heat pump applications. Although successful in eliminating stratospheric ozone depletion, HFCs possess a high global warming potential (GWP), exceeding thousands of times that of CO_2 in some cases.[1,2] Their replacement with hydrofluoroolefins (HFOs), with very low GWP, is underway; however, HFCs continue to be produced in large volumes and are frequently blended to meet performance requirements. The management of these refrigerants at the end of life has become a central environmental issue since current treatment routes are mostly limited to incineration, thereby losing their material value and generating further emissions.

A transition toward circular economy strategies demands the development of processes that enable the selective recovery and reuse of fluorinated gases (F-gases).[3,4] The challenge lies in separating compounds with very similar volatilities, as in commercial mixtures such as R410A, R407F, and R404C, where conventional cryogenic distillation becomes prohibitively energy-intensive. Various strategies have been proposed to address this challenge. Adsorption using activated carbons has been explored for its simplicity and low energy demand,[5−8] while membrane-based separation processes offer continuous operation and compact design.[9] In parallel, absorption using ionic liquids (ILs)[10−14] and deep eutectic solvents (DESs)[15] have emerged as a promising alternative, owing to their negligible vapor pressure and chemical tunability. Among these, fluorinated ionic liquids (FILs) stand out due to their capacity to enhance interactions with F-gases through the presence of fluorinated domains.[16] FILs display a remarkably high absorption capacity, mainly resulting from the increased free volume associated with their larger molecular structures.[17] Moreover, their regeneration is relatively simple due to the repulsive interactions introduced by the fluorine atoms,[18] which enhance their potential as promising solvents for F-gas recovery processes. Pereiro and co-workers have played a pioneering role in this area, being among the first to propose

Received: October 9, 2025
Revised: November 19, 2025
Accepted: November 21, 2025
Published: November 27, 2025

https://doi.org/10.1021/acs.jced.5c00660
J. Chem. Eng. Data 2025, 70, 4939−4953

and systematically investigate FILs as alternative solvents for gas separation and related applications.[19] Their studies have covered the synthesis and characterization of diverse families of FILs; the measurement of key properties such as density, viscosity, and surface tension; and the evaluation of gas solubilities and selectivities, particularly for fluorinated refrigerants and CO_2.[14,20] This body of work has provided a broad and solid experimental basis, highlighting both the opportunities and the challenges associated with FILs.

Despite these encouraging experimental findings, the identification of the most effective solvents remains largely empirical with limited molecular-level guidance. Indeed, reliable data on properties such as solubility, absorption enthalpy, or viscosity are essential to design an adequate industrial unit. Solubility determines the overall capacity of the solvent to capture the target HFC under specific temperature and pressure conditions, directly influencing the size of the equipment and its operational efficiency. The absorption enthalpy governs the energy required for solvent regeneration and thus defines the thermodynamic efficiency of the process, as low enthalpic penalties are desirable to minimize the thermal duty and operating costs of the desorption stage. Finally, viscosity plays a crucial role in the mass-transfer performance, affecting pumping requirements, contactor design, and cycle time.[21,22] In this regard, the use of computational tools based on accurate and predictive thermodynamic and transport models becomes extremely useful for expanding knowledge of thermophysical properties, particularly when limited experimental data are available.

In recent years, DFT approaches, such as the COnductor-like Screening MOdel for Real Solvents (COSMO-RS) and molecular-based equations of state (EoS) have been employed to establish predictive structure−property relationships, accelerating solvent screening and design. In this direction, Sosa et al.[23] presented a COSMO-based/Aspen Plus methodology to evaluate the performance of FILs/ILs as absorbents in the process scale of two F-gases, R134a and R32. In a subsequent publication,[24] they presented a comprehensive molecular screening and experimental validation strategy for designing ILs that capture hydrofluorocarbons, evaluating the solubility of more than 600 ILs. Apart from COSMO-RS, SAFT-type approaches have proven to be valuable in this regard, as they incorporate explicit molecular descriptors for chain connectivity, association, and polarity. In particular, the soft-SAFT EoS[25] has been extensively used to model the solubility of refrigerants in FILs[26,27] and DESs,[28,29] obtaining an excellent description of these systems, typically using two binary parameters. However, apart from the soft-SAFT version, limited work has been carried out using other SAFT approaches.

In particular, the Statistical Associating Fluid Theory with variable-range Mie potentials (SAFT-VR Mie)[30] stands as an interesting alternative, as it provides additional flexibility by tuning the repulsive and attractive exponents, which improves the representation of fluorinated systems with strong repulsive interactions. Although SAFT-VR Mie has been successfully applied to many systems, including the study of mixtures of refrigerants,[31] the solubility of HFCs in fluorinated ionic liquids remains limited to the most common anions. For example, Chiko et al.[32] compared the SAFT-VR Mie and CP-PC-SAFT models to describe the VLE, VLLE, critical loci, and saturated phase densities of a wide variety of gases, including HFCs in ILs with 1-alkyl-3-methylimidazolium ($[C_n\text{mim}]^+$) cations and bis(trifluoromethylsulfonyl)imide ($[Tf_2N]^-$), tetrafluoroborate ($[BF_4]^-$), and hexafluorophosphate ($[PF_6]^-$) anions. However, the description of long fluorinated anion chains containing more than four carbons has never been explored with SAFT-VR Mie.

The present work addresses this gap by developing SAFT-VR Mie molecular models for the solubility of the most representative HFCs, R32, R134a, and R125, in a series of ILs based on the 1-ethyl-3-methylimidazolium and 1-ethyl-3-methylpyridinium cations, combined with different anions exhibiting varying degrees of fluorination. The framework enables an assessment of the role of polarity and fluorine content in solubility and selectivity. These models are then used to describe the physicochemical behavior of these fluids when present in commercial blends to evaluate the capacity of the ILs for recovery and separation purposes. Their performance in terms of absorption capacity, as well as viscosity calculations through the implementation of the Helmholtz scaling theory, and the energy requirements, estimated via the enthalpy of regeneration of these systems, are outlined to provide insights into the design of solvent-based recovery processes that are compatible with circular economy objectives.

COMPUTATIONAL METHODS

Molecular-Based Equation of State: SAFT-VR Mie. The thermophysical properties of all systems analyzed in this work were modeled using the molecular-based SAFT-VR Mie equation of state (EoS),[30] which represents an advanced reformulation of the statistical associating fluid theory (SAFT) originally developed by Chapman and co-workers.[33] SAFT-VR Mie combines the rigor of statistical mechanics from the SAFT family with a Mie potential to represent dispersive and repulsive interactions more accurately across a broad range of conditions. As with any SAFT-type equation, the model is written in terms of Helmholtz free energy, A, which is decomposed into several molecular-level contributions that account for different types of interactions and structural effects within the fluid:

$$\frac{A}{Nk_BT} = \frac{A^{ig}}{Nk_BT} + \frac{A^{mono}}{Nk_BT} + \frac{A^{chain}}{Nk_BT} + \frac{A^{assoc}}{Nk_BT} + \frac{A^{pol}}{Nk_BT} \quad (1)$$

where N is Avogadro's number, k_B is the Boltzmann constant, and T is the absolute temperature. Each term represents a distinct physical contribution: the ideal gas term (A^{ig}), monomeric segment interactions (A^{mono}), chain formation (A^{chain}), association between specific sites due to hydrogen-bonding or similar directional interactions (A^{assoc}), and the effect of molecular polarity (A^{pol}).[30,34,35] This structure, based on additive physical effects, allows SAFT-VR Mie to describe, within a unified framework, both simple nonassociating fluids and complex associating or polar compounds.

The SAFT-VR Mie approach employs a generalized Mie potential to represent the dispersion and repulsion forces between spherical segments. This potential is fully characterized by four molecular parameters: the segment diameter (σ), the dispersion energy (ε/k_B), and the repulsive (λ_r) and attractive (λ_a) exponents. In most applications, λ_a is fixed at 6, while λ_r is molecule-dependent and is obtained through parameter fitting. Nonassociating and nonpolar species are

https://doi.org/10.1021/acs.jced.5c00660
J. Chem. Eng. Data 2025, 70, 4939−4953

therefore described by four parameters in total: the segment number (m_s), corresponding to the chain term, and the three Mie potential parameters σ, ε/k_B, and λ_r.

For associating fluids, two additional parameters are required: the site−site interaction energy (ε^{AB}) and the association range (r_c^{AB}), together with the specification of the association scheme. The latter can be expressed according to the original Huang and Radosz formalism[36] or in a compact notation that defines the number of bipolar (B), positive (P), and negative (N) sites per molecule.[37] When molecular polarity plays a significant role, further parameters are included to describe the permanent dipole moment (μ_{pol}) and the number of polar sites (n_{pol}). These extensions enable the model to reproduce complex thermodynamic behavior arising from dipole−dipole or hydrogen-bonding interactions.

The extension of the SAFT-VR Mie EoS to mixtures is conceptually straightforward, as the same molecular framework is applied to each component. However, accurate representation of the mixture behavior requires proper treatment of cross-interactions between unlike molecules. This is achieved by introducing a single binary interaction parameter, k_{ij}, which modifies the dispersion energy between dissimilar species to capture nonideal effects. The cross parameters, namely, the repulsive exponent (λ_{ij}), the segment diameter (σ_{ij}), and the dispersion energy (ε_{ij}), are evaluated using standard combining rules, as detailed below.

$$(\lambda_{ij} - 3) = \sqrt{(\lambda_{ii} - 3)(\lambda_{jj} - 3)} \tag{2}$$

$$\sigma_{ij} = \frac{(\sigma_{ii} + \sigma_{jj})}{2} \tag{3}$$

$$\varepsilon_{ij} = \sqrt{\varepsilon_{ii}\varepsilon_{jj}} \frac{\sqrt{(\sigma_{ii}\sigma_{jj})^3}}{\sigma_{ij}^3}(1 - k_{ij}) \tag{4}$$

Here, k_{ij} is obtained by fitting experimental vapor−liquid equilibrium (VLE) data for the absorption of the binary systems. This parameter was determined by minimizing the following objective function:

$$\mathrm{OF}(k_{ij}) = w_x \sum_{j=1}^{n} \left[\sum_{i=1}^{2} (x_{i,j}^{cal} - x_{i,j}^{exp})^2 \right] + w_p \sum_{j=1}^{n} \left[\frac{P_j^{cal} - P_j^{exp}}{P_j^{exp}} \right] \tag{5}$$

For bubble point calculations, n denotes the number of experimental data points, x_i is the liquid-phase mole fraction of component i, and P is the bubble pressure. Superscripts *cal* and *exp* represent the calculated and experimental values, respectively. The weighting factors for the liquid composition and dew pressure errors are denoted w_x and w_P, respectively. Summations are taken over all components ($c = 2$).

Phase equilibrium calculations within the SAFT framework are performed by imposing the classical thermodynamic equilibrium conditions and the equality of temperature, pressure, and chemical potential for each component in all coexisting phases. Once these conditions are satisfied, the equation of state provides a consistent description of the Helmholtz free energy of the system from which any derived thermodynamic property (e.g., density, enthalpy, or vapor−liquid equilibrium composition) can be obtained. The calculations were performed using the open source code SGTPy.[38]

Helmholtz Scaling Theory for Viscosity. The dynamic viscosity of pure fluids was evaluated using the Helmholtz scaling theory (A-scaling) proposed by Tavares and his research team,[39] in which the residual Helmholtz free energy is calculated from the SAFT-VR Mie equation of state, following a similar approach to that applied in previous work.[40] The approach is based on defining an ansatz function that depends on the difference between the molar Helmholtz energy of the fluid, $\bar{A}$, and the corresponding hard-sphere reference, $\bar{A}_{HS}$. Accordingly, the viscosity is expressed as

$$\ln\left(\frac{\eta}{\eta^{HS}}\right) = f\left(\Psi\left[\left(\frac{\bar{A}}{RT}\right) - \left(\frac{\bar{A}_{HS}}{RT}\right)\right]\right) = f\left(\frac{\Psi\bar{A}^*}{RT}\right) \tag{6}$$

Here, $\bar{A}$ is obtained from the SAFT-VR Mie formalism, while $\bar{A}_{HS}$ corresponds to the hard-sphere contribution, already included in the monomer term (A^{MONO}). The scaling factor Ψ is defined as a function of reduced temperature, $T^* = k_B T/\varepsilon$, namely $\Psi = (T^*)^\theta$, with θ being an empirical, fluid-specific constant. In eq 6, η^{HS} denotes the viscosity of a hard-sphere fluid, calculated from the Chapman−Enskog relation:

$$\eta^{HS} = \frac{5}{16} \frac{\sqrt{\frac{MT\varepsilon}{N_{av}\pi}}}{\sigma^2 \boldsymbol{\Omega}^{(2,2)}} \tag{7}$$

where the collision integral $\boldsymbol{\Omega}^{(2,2)*}$ is obtained from the Neufeld correlation.[41] For pure fluids, the original ansatz function f is expressed as a cubic polynomial in terms of $(\Psi\bar{A}^*/RT)$:

$$\ln\left(\frac{\eta}{\eta^{HS}}\right) = a + b\left(\frac{\Psi\bar{A}^*}{RT}\right) + c\left(\frac{\Psi\bar{A}^*}{RT}\right)^2 + d\left(\frac{\Psi\bar{A}^*}{RT}\right)^3 \tag{8}$$

where coefficients a, b, c, and d are pure-component parameters obtained by fitting the model to the experimental viscosity data of the ILs. In contrast to the original formulation and its ansatz function, only three parameters (θ, a, and b) were necessary to achieve an accurate correlation of the IL viscosities in this work.

RESULTS AND DISCUSSION

Molecular Models. In this work, six ILs, based on the 1-ethyl-3-methylimidazolium or pyridinium cations, in combination with anions containing a diverse number of fluorine atoms, were studied. For a practical analysis, anions with three fluorine atoms, such as triflate $[CF_3SO_3]^-$, six fluorine atoms, such as bis(trifluoromethylsulfonyl)imide $[(CF_3SO_2)_2N]^-$ or $[Tf_2N]^-$, and nine fluorine atoms, such as perfluorobutanesulfonate $[C_4F_9SO_3]^-$ and perfluoropentanoate $[C_4F_9CO_2]^-$, were studied. The full list of chemical names and their formulas is summarized in Table 1.

All ILs were modeled using the ion-pair assumption, treating the cation and anion as a single molecular entity and therefore assigning a single set of molecular parameters to the combined species. This assumption is typically made in other modeling SAFT contributions[26,27] and is based on the short lifetime where anions and cations are alone in the system, reducing the ionic character of ILs, as observed in molecular simulations.[42] This approach keeps the model at a lower degree of complexity without losing accuracy when modeling vapor−liquid equi-

https://doi.org/10.1021/acs.jced.5c00660
J. Chem. Eng. Data 2025, 70, 4939−4953

Table 1. Summary of the Ionic Liquids and Refrigerants Investigated in This Work[a]

chemical name	chemical formula	CASRN
1-ethyl-3-methylimidazolium trifluoromethanesulfonate	$[C_2mim][CF_3SO_3]$	145022-44-2
1-ethyl-3-methylimidazolium bis(trifluoromethylsulfonyl)imide	$[C_2mim][Tf_2N]$	174899-82-2
1-ethyl-3-methylimidazolium perfluorobutanesulfonate	$[C_2mim][C_4F_9SO_3]$	NA
1-ethyl-3-methylimidazolium perfluoropentanoate	$[C_2mim][C_4F_9CO_2]$	NA
1-ethyl-3-methylpyridinium perfluorobutanesulfonate	$[C_2mpy][C_4F_9SO_3]$	1015420-87-7
1-ethyl-3-methylpyridinium perfluoropentanoate	$[C_2mpy][C_4F_9CO_2]$	NA
difluoromethane (R32)	CH_2F_2	75-10-5
1,1,1,2-tetrafluoroethane (R134a)	CH_2FCF_2	811-97-2
pentafluoroethane (R125)	CHF_2CF_3	354-33-6

[a]All compounds were modeled with the SAFT-VR Mie equation of state and the Helmholtz scaling theory.

libria, where the IL behaves effectively as a single, nonvolatile component.

The electrostatic delocalization of the anion, particularly due to the presence of fluorine atoms, plays a crucial role in defining the association scheme. In SAFT-VR Mie, the dominant cation−anion interaction is described through a bipolar site, which accounts simultaneously for the donor−acceptor nature of the ion pair. In addition to this bipolar site, negative sites are used to represent the delocalization of charge in the anion, mainly associated with the presence of fluorine and oxygen atoms. Accordingly, $[C_2mim][Tf_2N]$, $[C_2mim][C_4F_9SO_3]$, $[C_2mpy][C_4F_9CO_2]$, $[C_2mpy][C_4F_9SO_3]$, and $[C_2mim][C_4F_9CO_2]$ are complemented by two negative sites that account for the delocalized regions of the anion. For $[C_2mim][Tf_2N]$, these sites correspond to the SO_2 groups surrounding the nitrogen atom; in $[C_2mim][C_4F_9SO_3]$ and $[C_2mpy][C_4F_9SO_3]$, they are linked to the SO_3 group, and in $[C_2mim][C_4F_9CO_2]$ and $[C_2mpy][C_4F_9CO_2]$, they are associated with the CO_2 group. For the particular case of $[C_2mim][CF_3SO_3]$, the anion has a more localized electrostatic potential than the previous ones but still presents a considerable region of charge concentration where association can occur. Therefore, apart from the bipolar site, one additional negative site has been added to ensure that its residual delocalization is captured. It is worth noting that the $[CF_3SO_3]^-$ anion has been previously modeled in other SAFT approaches using a single bipolar site only;[26,43] however, here, the inclusion of an extra negative site improves the representation of its associative behavior. Cross association between unlike FILs is restricted to bipolar−negative or bipolar−bipolar interactions, depending on the anion structure, consistent with quantum-chemical calculations and spectroscopic evidence. A graphical representation of the coarse-grained models used to represent these ILs is provided in Figure 1.

The SAFT-VR Mie parameters were determined by fitting them to experimental liquid-phase density data (ρ_l) over a range of temperatures and pressures. Each molecular parameter set (ξ) was optimized by minimizing the deviations between experimental and calculated densities using the following objective function (OF):

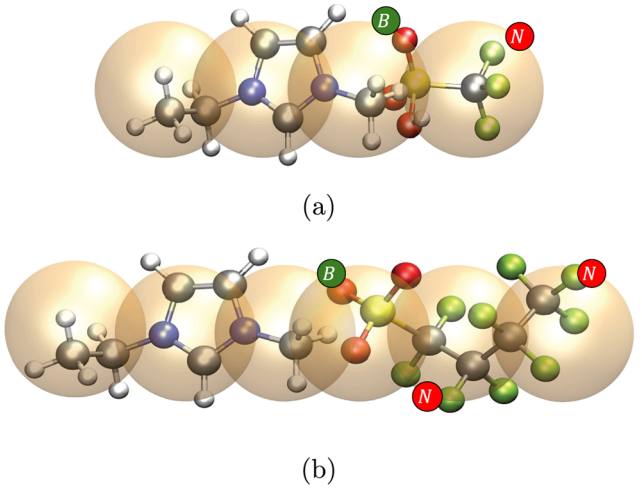

Figure 1. Graphical representation of the molecular parametrization for (a) $[C_2mim][CF_3SO_3]$ and (b) $[C_2mim][C_4F_9SO_3]$ according to the SAFT-VR Mie equation of state. Red circles denote negative association sites, while green circles denote bipolar sites. The molecular representations of $[C_2mim][Tf_2N]$, $[C_2mim][C_4F_9CO_2]$, $[C_2mpy][C_4F_9SO_3]$, and $[C_2mpy][C_4F_9CO_2]$ follow the same association scheme as $[C_2mim][C_4F_9SO_3]$.

$$\mathrm{OF}(\xi) = \frac{1}{n}\sum_{i=1}^{n}\left(\frac{\rho_{l,i}^{\mathrm{cal}}}{\rho_{l,i}^{\mathrm{exp}}} - 1\right) \tag{9}$$

A summary of the resulting SAFT-VR Mie molecular parameters is given in Table 2, along with the absolute average deviation (%AAD) calculated from eq 9. The analysis of the molecular parameters revealed some interesting trends. First, the molecular volume $m_s\sigma^3$ is clearly correlated with the size of each IL, as shown in Figure S1. This behavior has also been observed in other SAFT approaches that have studied these ILs.[43] Moreover, the chain length m_s was kept at the same value for the two pairs of ILs sharing the anion, with minor volume differences being corrected by σ. In both cases, the pyridinium cation provides slightly higher diameters than the imidazolium one. In terms of energy, $[C_2mim][CF_3SO_3]$ displayed the highest value, with a notable difference compared to the rest of the compounds. This comes at the cost of lower values of association, clearly indicating a lower capacity to form association bonds, while its strong van der Waals energy is probably due to its relatively smaller but bulkier structure, compared to the rest of the compounds. A similar feature was found in the literature using the soft-SAFT EoS.[26] The second-highest dispersive energy corresponded to the $[Tf_2N]$ anion, while the rest of the FILs showed lower values, as a consequence of a longer anion length and a very symmetric distribution of the fluorine atoms. It is believed that steric effects play a role, slightly decreasing the energy of interaction. No substantial differences were found between the four FILS, although the presence of a sulfonate (SO_3^-) provides a slightly lower energy of association than the perfluoropentanoate anion $[C_4F_9CO_2]^-$.

Figure 2a,b depicts the description of the density as a function of pressure for $[C_2mim][CF_3SO_3]$ and $[C_2mim][Tf_2N]$, respectively. As can be seen, an excellent description can be achieved for all isotherms over the whole range of pressures, without exhibiting any deterioration. In both cases, the relative error in density remains around 0.03%, which is

https://doi.org/10.1021/acs.jced.5c00660
J. Chem. Eng. Data 2025, 70, 4939−4953

Table 2. SAFT-VR Mie Molecular Parameters for the Studied Ionic Liquids and Refrigerants[a]

ionic liquid	MW (g/mol)	m_s	σ, Å	ε/k_B, K	λ_r	ε^{AB}, K	r_c^{AB}	[B,P,N]	$\%AAD_{\rho_L}$
$[C_2mim][CF_3SO_3]$	260.24	4.602	3.996	460.285	14.397	1720.19	0.1840	[1,0,1]	0.030
$[C_2mim][Tf_2N]$	391.31	6.414	3.945	392.794	13.594	2793.93	0.2135	[1,0,2]	0.033
$[C_2mim][C_4F_9SO_3]$	410.31	6.226	4.023	370.503	13.616	2864.25	0.3199	[1,0,2]	0.018
$[C_2mim][C_4F_9CO_2]$	374.21	6.167	3.939	328.132	12.976	3054.92	0.3968	[1,0,2]	0.017
$[C_2mpy][C_4F_9SO_3]$	421.28	6.226	4.090	377.763	13.976	2864.25	0.3259	[1,0,2]	0.030
$[C_2mpy][C_4F_9CO_2]$	385.23	6.167	3.993	276.532	10.447	3324.017	0.412	[1,0,2]	0.012
HFC	MW (g/mol)	m_s	σ, Å	ε/k_B, K	λ_r	μ_{pol} (D)	n_{pol}	reference	
R134a	102.030	2.448	3.401	220.634	14.672	2.058	0.711	44	
R32	52.023	2.422	2.835	159.060	10.479	1.978	0.782	44	
R125	120.021	1.940	3.796	261.211	19.915	1.563	0.310	44	

[a] λ_a and r_d^{AB}/σ are fixed for all pure fluids to 6 and 0.4, respectively.

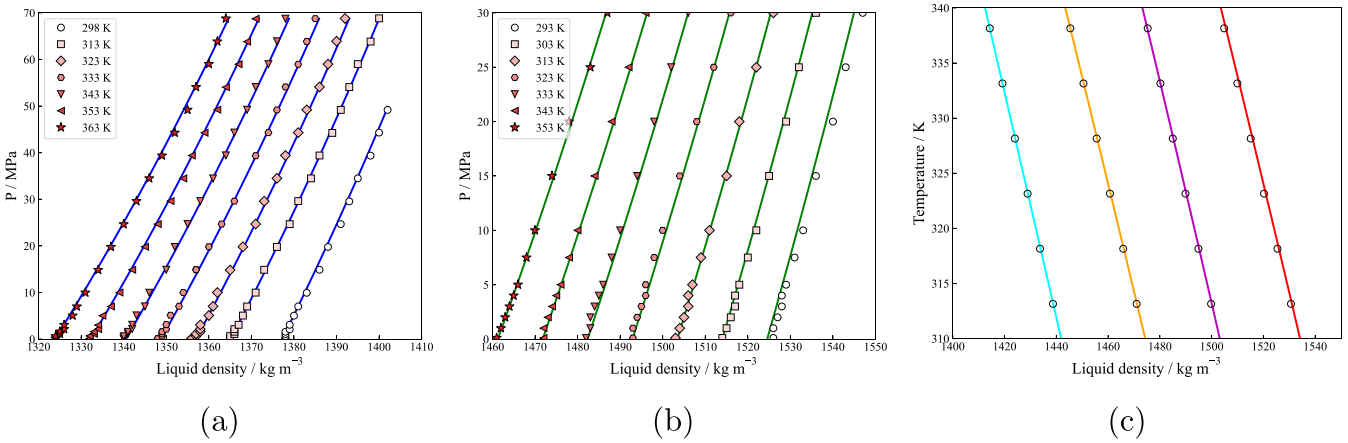

Figure 2. Single-phase density of (a) $[C_2mim][CF_3SO_3]$[45] and (b) $[C_2mim][Tf_2N]$[46] at different isotherms and (c) $[C_2mim][C_4F_9SO_3]$ (red —),[47] $[C_2mim][C_4F_9CO_2]$ (orange —),[47] $[C_2mpy][C_4F_9SO_3]$ (pink —),[19] and $[C_2mpy][C_4F_9CO_2]$ (blue —)[48] at atmospheric pressure. Symbols represent experimental data, and lines indicate SAFT-VR Mie calculations.

remarkable considering the wide range of conditions evaluated. In Figure 2c, the density of the remaining FILs, $[C_2mim][C_4F_9SO_3]$, $[C_2mim][C_4F_9CO_2]$, $[C_2mpy][C_4F_9SO_3]$, and $[C_2mpy][C_4F_9CO_2]$, is also displayed as a function of temperature and atmospheric pressure. Following the same trend as before, the density is perfectly reproduced with the proposed set of parameters, with an %AAD below 0.03%.

Table 2 also includes the parameters for the refrigerants, R32, R125, and R134a, which were modeled by considering only the polar contribution, as their molecular structures exhibit significant permanent dipole moments due to the presence of highly electronegative fluorine atoms, as shown in the literature with different SAFT versions integrating this term.[31,49] Further details and a rational analysis of the results for the pure refrigerants can be found in a recent contribution.[44]

Apart from the density, the viscosity of these ILs (with the exception of $[C_2mpy][C_4F_9CO_2]$, as no experimental data were found) was also modeled using the Helmholtz scaling theory. The description of the viscosity at different temperatures and atmospheric pressures is shown in Figure 3. As it can be observed, the exponential behavior of the viscosity is perfectly reproduced, reaching excellent agreement with the available experimental data,[19,47,50] even at high viscosity values, with all relative errors below 0.5% (see Table 3). Furthermore, it is notable that an accurate prediction was carried out with only three adjustable parameters.

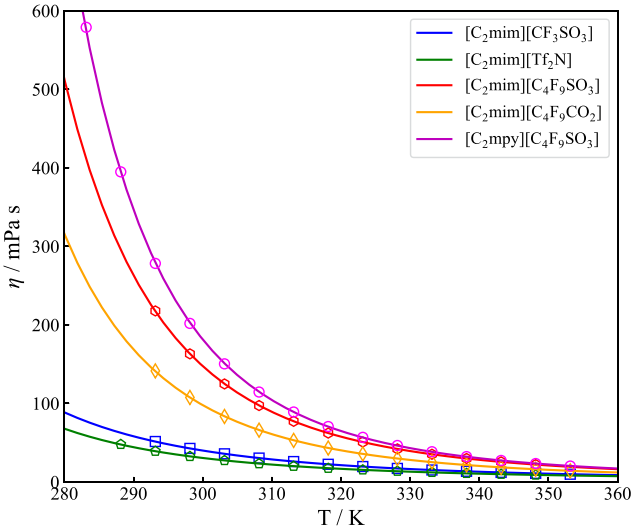

Figure 3. Liquid viscosities of the studied ILs at atmospheric pressure. Symbols denote experimental data,[19,47,50] while the full lines correspond to the fitting using the Helmholtz scaling theory coupled with the SAFT-VR Mie EoS.

Solubility of HFCs in ILs. Following the parametrization of the selected FILs, the solubility of the studied HFCs in these compounds is described using SAFT-VR Mie. In order to achieve an accurate description, a binary parameter k_{ij} was used

https://doi.org/10.1021/acs.jced.5c00660
J. Chem. Eng. Data 2025, 70, 4939−4953

Table 3. Fitted Parameters of the Helmholtz Scaling Theory (θ, a, and b) for the Studied ILs[a]

	θ	a	b	%AAD
$[C_2mim][CF_3SO_3]$	−0.913	5.366	−0.118	0.145
$[C_2mim][Tf_2N]$	−1.234	5.618	−0.093	0.491
$[C_2mim][C_4F_9SO_3]$	−1.459	5.854	−0.131	0.131
$[C_2mim][C_4F_9CO_2]$	−1.432	5.557	−0.164	0.250
$[C_2mpy][C_4F_9SO_3]$	−1.855	6.143	−0.114	0.368

[a]The parameters were obtained by regression to experimental viscosity data, and the last column reports the absolute average deviation (%AAD) between experimental and fitted values.

Table 4. List of k_{ij} Binary Parameters for All of the Working Pairs Involved in This Fluid[a]

	R134a	R32	R125	%AAD
$[C_2mim][CF_3SO_3]$	−0.0080	−0.0337	−0.0273	7.017
$[C_2mim][Tf_2N]$	−0.0169	−0.0453	−0.0260	6.281
$[C_2mim][C_4F_9SO_3]$	−0.0157	−0.0468	−0.0416	5.457
$[C_2mim][C_4F_9CO_2]$	−0.0174	−0.0464	−0.0514	2.335
$[C_2mpy][C_4F_9SO_3]$	−0.0148	−0.0535	−0.0433	2.411
%AAD	4.426	2.643	5.228	4.121

[a]Values are temperature-independent.

to better adjust the solubility behavior across the entire experimental data range.

In Figure 4, the solubility of R32, R125, and R134a in FILs with nine fluorine atoms at a constant temperature of 303.15 K is plotted. The agreement between the experimental data[14] and the SAFT-VR Mie model is excellent using a single binary parameter (see Table 4). Here, it is very important to note that all of the k_{ij} values are very close to zero, indicating that only slight corrections are necessary to describe these highly complex systems. In particular, the description of the solubility of R134a can even be done without any correction, as all values remain around a very modest $k_{ij} = -0.01$. The highest values are around $k_{ij} = -0.05$ and correspond to the solubility of R32. All parameters are negative, indicating that the predicted values ($k_{ij} = 0$) slightly underestimate the solubility of the HFCs in these FILs. Here, it is important to remark that the model explicitly considers polarity in the refrigerants and association in the FILs but does not include any type of association in the HFCs, as it had been done in the previous literature.[16,26] The current model presents a more realistic picture of the dipolar nature of the refrigerant and, at the same time, is capable of

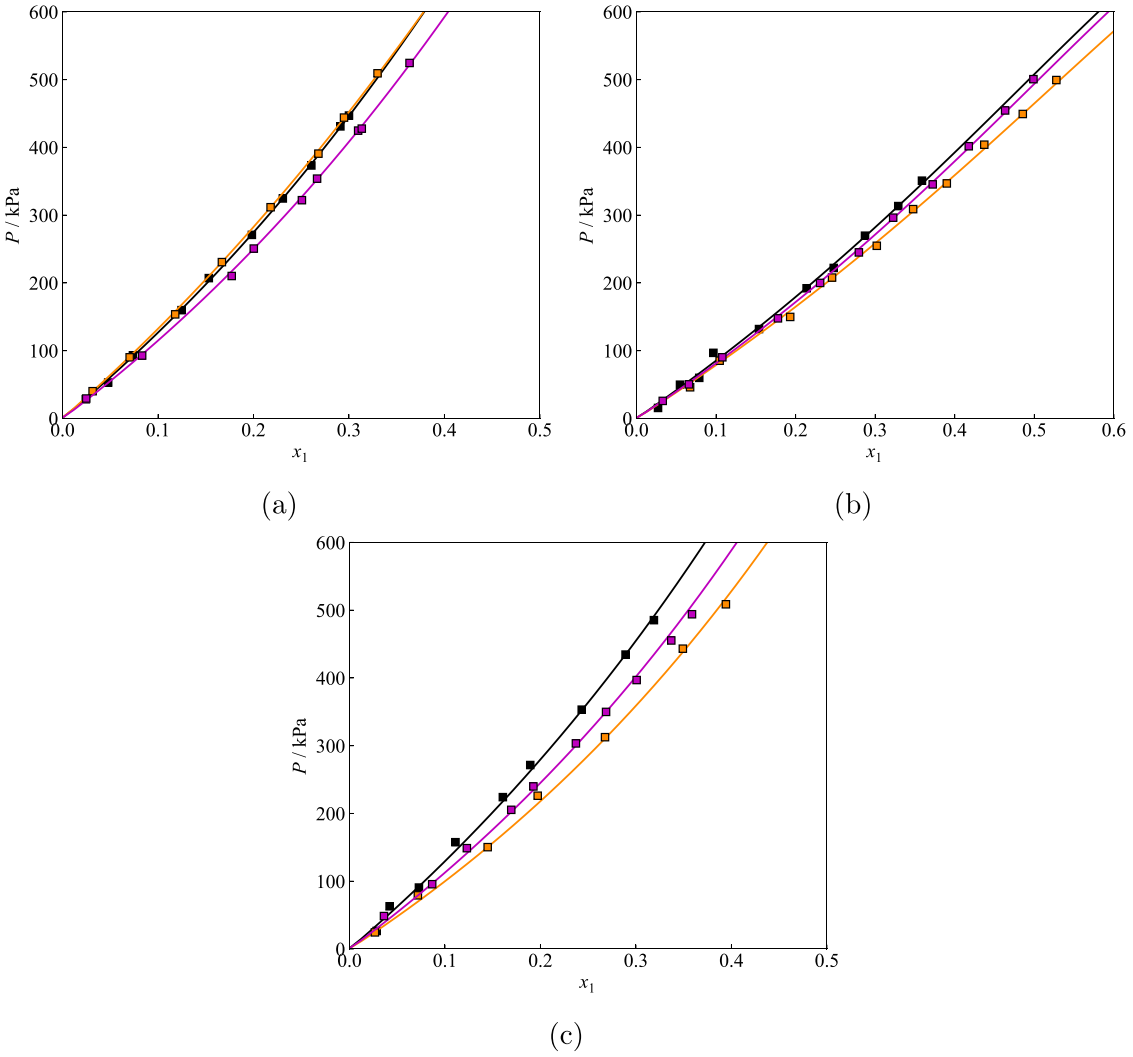

Figure 4. Pressure−composition (P−x_1) diagrams for (a) R32, (b) R134a, and (c) R125 in $[C_2mim][C_4F_9SO_3]$(blue), $[C_2mim][C_4F_9CO_2]$-(orange), and $[C_2mpy][C_4F_9SO_3]$(magenta) at 303.15 K. Symbols denote experimental data,[14] and lines correspond to the SAFT-VR Mie model.

https://doi.org/10.1021/acs.jced.5c00660
J. Chem. Eng. Data 2025, 70, 4939−4953

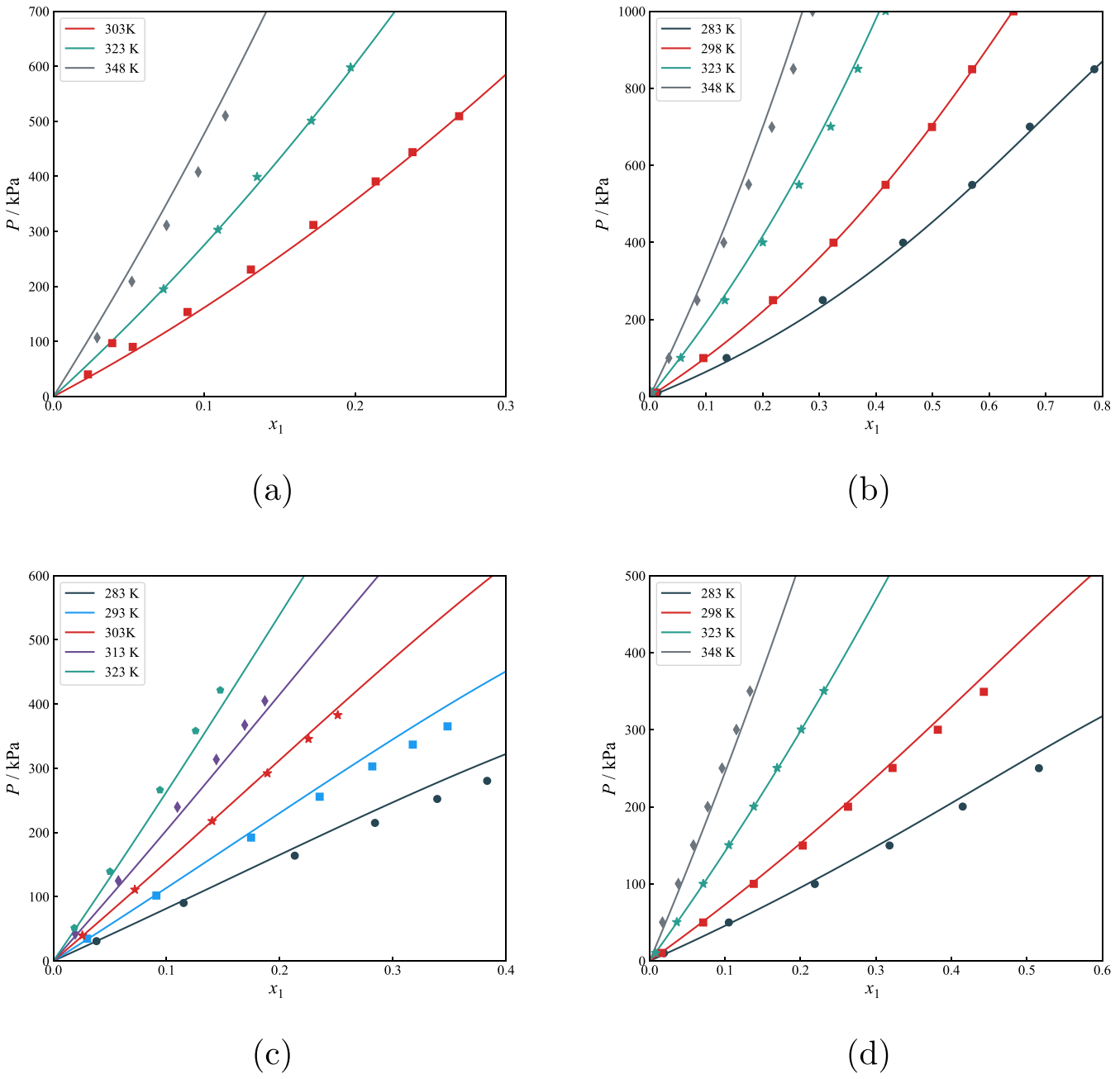

Figure 5. Pressure−composition (P−x_1) diagrams at different isotherms for (a) R32 in [C_2mim][CF_3SO_3], (b) R32 in [C_2mim][Tf_2N], (c) R134a in [C_2mim][CF_3SO_3], and (d) R134a in [C_2mim][Tf_2N]. Symbols denote experimental data,[10,11,13,51] and lines correspond to the SAFT-VR Mie model.

capturing the interactions between these molecules and the ILs. It is worth noting that previous soft-SAFT studies employed an associating model for HFCs with two binary interaction parameters, whereas in this work, SAFT-VR Mie uses an explicit polar term and a single temperature-independent binary interaction parameter. While both approaches are capable of adequately describing these systems, a quantitative comparison would be misleading due to the different balances among dispersion, association, and polarity provided by the two models.

Unfortunately, current experimental data are only available at 303.15 K for the studied FILs. This does not allow us to check whether the current k_{ij} is able to predict the behavior of these FILs at other temperatures. For this purpose, the solubility of R134a and R32 in the more common [C_2mim]-[CF_3SO_3] and [C_2mim][Tf_2N] ILs was also modeled at different temperatures using a single k_{ij}. The results are plotted in Figure 5.

The results obtained are encouraging, as the description of these systems at different temperatures provides excellent agreement with the available data using a temperature-independent k_{ij} binary parameter (see Table 4), whose values are within the same range as those of the previous FILs. This fact is particularly important when modeling a separation process, where the desorption step can be carried out at higher temperatures, and data are not available. In addition, it highlights the capacity of the model to capture the behavior of these solvents regardless of the number of fluorine atoms they

https://doi.org/10.1021/acs.jced.5c00660
J. Chem. Eng. Data 2025, 70, 4939−4953

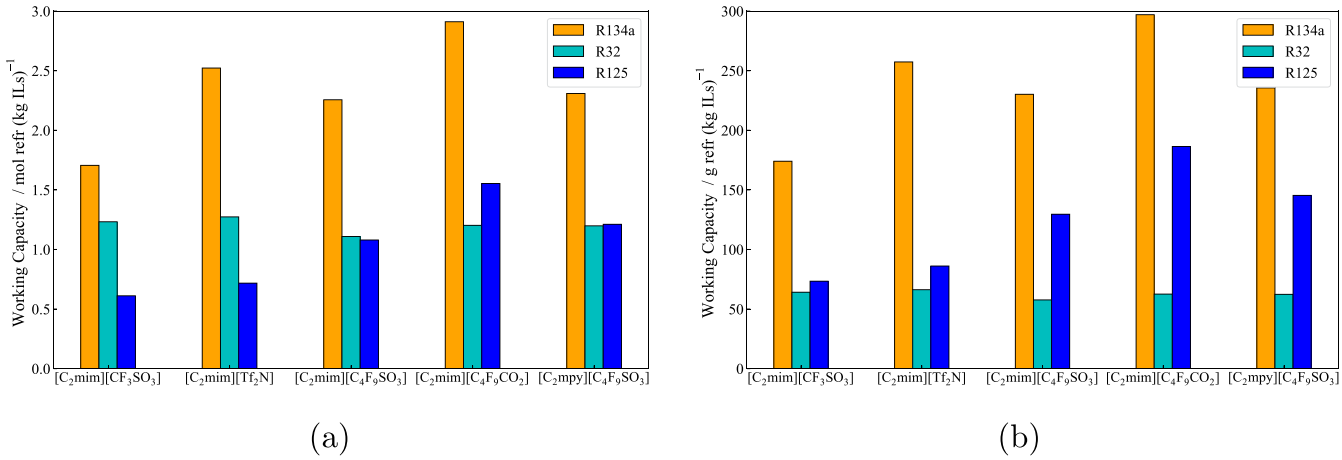

Figure 6. Working capacity of R134a (orange), R32 (light blue), and R125 (blue) in the five studied solvents in (a) moles of refrigerant absorbed per kilogram of solvent and (b) grams of refrigerant absorbed per kilogram of solvent. Absorption was carried out at 5 bar and T = 303.15 K, while desorption was conducted at atmospheric pressure and T = 343.15 K.

contain, as no degeneracy in the results is observed (higher values of k_{ij} denote stronger corrections). The solubility of R125 in [C$_2$mim][CF$_3$SO$_3$] and [C$_2$mim][Tf$_2$N] also exhibits good agreement with the experimental data and is graphically displayed in Figure S2.

Based on the accurate results obtained for the [CF$_3$SO$_3$] and [Tf$_2$N] anions, and the similar k_{ij} values compared to the FILs of Figure 4, it is believed that predictions at other temperatures will also provide accurate values for these fluids. This allows for exploring their real capacity to be used in refrigeration applications (recovery of refrigerants, absorption refrigeration cycles, etc.). Consequently, the working capacity (WC) of all FILs for the three studied HFCs was estimated. As a benchmark case, a recovery unit prototype working at 5 bar and 303.15 K was used for absorption, while desorption was carried out at atmospheric pressure and 343.15 K. It should be noted that the high-temperature calculations are purely predictive due to the absence of experimental measurements. The working capacity (WC) can be defined as the difference in mass or mole solubility between the two conditions.

$$\mathrm{WC} = w_i(P_{\mathrm{abs}}, T_{\mathrm{abs}}) - w_i(P_{\mathrm{des}}, T_{\mathrm{des}}) \tag{10}$$

A relevant consideration when discussing WC is the selection of units. Although EoS models usually report solubilities in mole fraction, which is the convention adopted in much of the literature, refrigeration processes are better evaluated on a mass basis from a practical standpoint. This is not a minor question, as it may lead to misleading conclusions. This is illustrated in Figure 6a, where the WC is expressed as moles of refrigerant per kilogram of solvent, compared to Figure 6b, where the WC is expressed as mass of refrigerant per kilogram of solvent.

In both figures, it is clearly observed that R134a is the HFC exhibiting the highest capacity to be captured by all of the ILs studied in this work, with a maximum value close to 2.9 mol or 300 g R134a/kg IL when using [C$_2$mim][C$_4$F$_9$CO$_2$]. [C$_2$mim][Tf$_2$N] stands out as the second best option, slightly surpassing 2.5 mol or 250 g R134a/kg IL. However, the analysis becomes trickier when evaluating the performance of R32 and R125. In moles of refrigerant terms, the WC of R32 is higher or similar to that of R125 in all cases, with the exception of [C$_2$mim][C$_4$F$_9$CO$_2$]. The situation is radically different when expressed in grams of refrigerant, with R125 exhibiting a higher capacity than R32 in all of the solvents studied. This is particularly important for applications in the separation of R32−R125 mixtures, such as in the case of the commercial blend R410A. In fact, while Figure 6a suggests a substantial difference in terms of WC when using the [CF$_3$SO$_3$]$^-$ anion, Figure 6b indicates a far better performance of [C$_4$F$_9$CO$_2$]$^-$ in terms of WC difference between R32 and R125.

Competitive Selectivity and Solubility in Commercial Blends. Although the ideal selectivity can be estimated from the binary solubility diagrams of individual refrigerants in ILs, this measure does not account for the competition between gases and therefore provides only a preliminary indication of the separation potential. A more realistic evaluation requires analyzing the competitive selectivity for recovering the components from multicomponent commercial refrigerant blends, such as R410A and R407F. This involves the evaluation of multicomponent mixtures at specific compositions. The competitive selectivity ($S_{i/j}$) of a specific HFC can be determined according to eq 11:

$$S_{i/j} = \frac{y_j/x_j}{y_i/x_i} \tag{11}$$

where x and y denote the mole fractions of the components in the liquid and gas phases, respectively.

In this work, we adopted an approach similar to that described in a previous contribution from Tavares and co-workers,[29] where the competitive selectivity is evaluated from vapor−liquid flash calculations using SAFT-VR Mie. The methodology solves the Rachford−Rice equation iteratively to obtain the equilibrium compositions of the refrigerant−IL mixtures at the desired operating conditions. The global feed composition was fixed to a molar fraction of z_{IL} = 0.7 for the IL and $z_{\mathrm{F\text{-}gas}}$ = 0.3 for the refrigerant blend (with the commercial proportions of each mixture).

Prior to this, it is necessary to accurately describe all of the binary systems involved in the process. While the description of the HFC−IL interactions is addressed in previous sections, the vapor−liquid equilibria for the binary blends R32−R125, R32−R134a, and R125−R134a were modeled using a temperature-independent k_{ij} fitted to available equilibrium pressure and composition experimental data,[52−54] consistent with previous calculations. The binary interaction parameter

https://doi.org/10.1021/acs.jced.5c00660
J. Chem. Eng. Data 2025, 70, 4939−4953

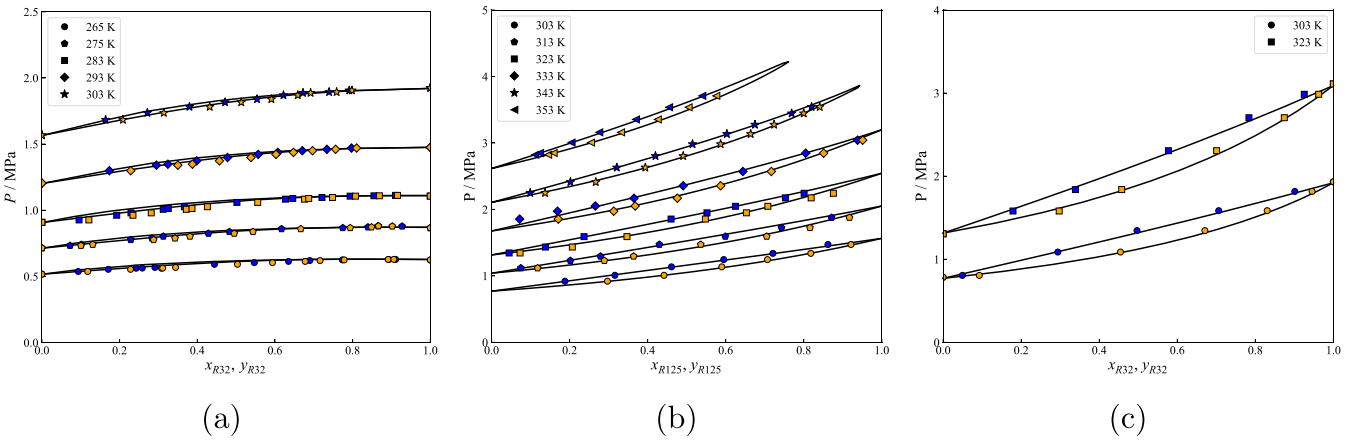

Figure 7. Vapor−liquid equilibrium (VLE) data for (a) R32 + R125, (b) R125 + R134a, and (c) R32 + R134a mixtures at different temperatures. Experimental data[52−54] are shown as blue and yellow markers for bubble and dew point compositions, respectively. Different marker shapes denote the corresponding temperatures indicated in the legend. Solid lines represent the phase envelopes calculated by using SAFT-VR Mie.

was determined by fitting vapor−liquid equilibrium data using the following equation,

$$\mathrm{OF}_{\mathrm{VLE}}(k_{ij}) = \sum_{j=1}^{n} \left\{ \sum_{i=1}^{c=2} [(x_{i,j}^{\mathrm{cal}} - x_{i,j}^{\mathrm{exp}})^2 + (y_{i,j}^{\mathrm{cal}} - y_{i,j}^{\mathrm{exp}})^2] + \left[\frac{P_j^{\mathrm{cal}} - P_j^{\mathrm{exp}}}{P_j^{\mathrm{exp}}} \right]^2 \right\} \tag{12}$$

where $x_{i,j}^{\mathrm{cal}}$ and $y_{i,j}^{\mathrm{cal}}$ represent the calculated liquid and vapor mole fractions of component i at point j, $x_{i,j}^{\mathrm{exp}}$ and $y_{i,j}^{\mathrm{exp}}$ are their experimental counterparts, and P_j^{cal} and P_j^{exp} correspond to the calculated and experimental saturated pressures, respectively.

The results of these models are shown in Figure 7, where the three binary systems are perfectly described with an AAD% below 0.13%. The required k_{ij} values are included in Table 5.

Table 5. List of k_{ij} Parameters for the Binary Mixtures of HFCs Involved in This Work

mixture	k_{ij}	%AAD
R32−R134a	−0.0179	0.038
R125−R134a	−0.0114	0.073
R32−R125	−0.0575	0.126

As can be seen, these values remain close to zero, again indicating that the SAFT-VR Mie model requires only minor corrections to provide quantitative agreement for these systems.

Based on the results of the WC, the competitive selectivity and solubility between the refrigerants were studied at conditions representing typical commercial blends using SAFT-VR Mie. In particular, the selectivity to separate R32 and R125 from a R410A commercial blend (a mixture containing 69.7 mol % R32 and 30.3 mol % R125) and the solubility of both compounds were evaluated at several isotherms as a function of pressure in $[C_2\mathrm{mim}][CF_3SO_3]$ and $[C_2\mathrm{mim}][C_4F_9CO_2]$. The same calculations for the rest of the ILs are plotted in Figure S3.

As can be seen in Figure 8a, the selectivity when using the $[CF_3SO_3]$ anion decreases almost linearly with pressure and temperature, although the impact of the pressure is smoothed as the temperature is increased. The values obtained remain close to 2. Figure 8b predicts the solubility of R32 and R125 in the same IL when present in an R410A blend and compares the results with the solubility when they are pure. In the mixture, it can be corroborated that R32 remains more soluble than R125. While the solubility fraction decreases in both cases, considering that they both compete for absorption, the differences in molar composition are more evident than when they are studied individually due to the higher amount of R32 (in moles) in the R410A system.

The results concerning the use of the $[C_4F_9CO_2]$ anion, plotted in Figure 8c, differ radically. In this case, the selectivity falls below 1, suggesting that R125 is more soluble than R32. The increase of pressure and temperature favors R32, which, in this case, means that the selectivity approaches 1. These results are in agreement with the observations of Figure 6a, provided that the selectivity is calculated based on mole fractions. However, the results in Figure 8d, which plots the competitive solubility between R32 and R125, show a higher proportion of R32 (full blue line) absorbed in the FIL, compared to R125 (full orange line). This would be the consequence of a higher amount of R32 in the system. According to these results, one could expect that the competitive selectivity remains above 1 in Figure 8c. After carefully reviewing these results, it has been noted that a greater amount of R32 is vaporized compared to R125, compensating the liquid phase fraction results and decreasing the selectivity according to the definition of eq 11.

As a result of this analysis, one must note that selectivity and solubility calculations should be carefully verified, considering the composition of the blend. For the particular case of R410A, whose molar R32 composition approaches 70%, a selectivity value of 2 will basically equal the amount of R32 and R125 absorbed in the IL (given that the R32/R125 ratio near the 70/30 proportion is close to 2), and the separation will not be favored.

A similar analysis was performed for the R407F refrigerant. This ternary blend contains 48.30 mol % R32, 20.13 mol % R125, and 31.57 mol % R134a. Consequently, the evaluation of the selectivity in pairs will provide only partial information. In Figure 9a, the selectivity of R32 over R125 is plotted when using $[C_2\mathrm{mim}][CF_3SO_3]$. In this case, the selectivity is similar to that seen in the R410A blend. This is due to the fact that the composition ratio between these two substances (2.40) is

https://doi.org/10.1021/acs.jced.5c00660
J. Chem. Eng. Data 2025, 70, 4939−4953

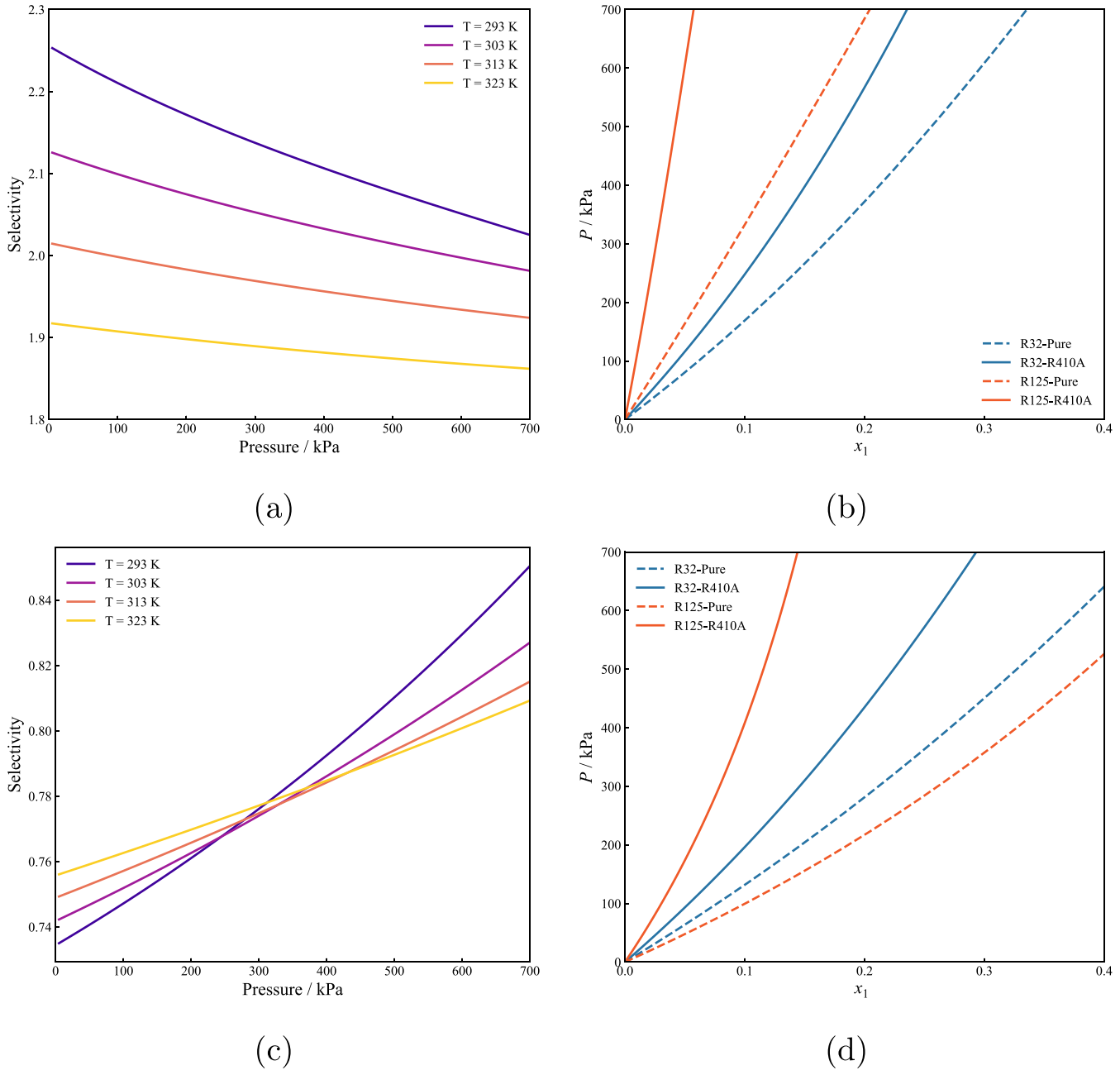

Figure 8. Analysis of the recovery of R32 from the R410A commercial blend. (a) Competitive selectivity of R32 over R125 at different isotherms, and (b) competitive absorption of R32 and R125 in the R410A blend at 303.15 K in $[C_2mim][CF_3SO_3]$. (c) Competitive selectivity of R32 over R125 at different isotherms and (d) competitive absorption of R32 and R125 in the R410A blend at 303.15 K in $[C_2mim][C_4F_9CO_2]$. Dashed lines represent the solubility of the HFCs in the selected ILs when they are being pure.

relatively similar to that of R410A (2.33). In all cases, the selectivity remains around 2 and decreases with pressure and temperature. When analyzing the selectivity of R32 with respect to R134a, the values remain slightly below 1. This indicates that R134a is apparently absorbed to a greater extent than R32. While this behavior is consistent with the information obtained from the WC (see Figure 6a), Figure 9c indicates that the solubility of R32 in an R407F mixture is slightly higher than that of R134a due to the large amount of the former HFC in the composition. As it happened for the R410A case in $[C_2mim][C_4F_9CO_2]$, the selectivity remains below 1 because of the effect of the vapor phase, where a higher amount of R32 is vaporized compared to R134a, compensating for the absorption of the liquid phase. This again highlights that multicomponent analysis is necessary to really understand all effects playing a role in the separation process. The selectivity results of R32 using $[C_2mim][C_4F_9CO_2]$ are plotted in Figure 9d,e. In both cases, the selectivity remains below 1, indicating that R32 has less affinity than R125 and R134a. Once again, this is caused by the role of the vapor phase in determining the solubility of the compounds in the mixture in Figure 9f. R125 exhibits the lowest absorption when mixed in the R407F proportion, but its presence in the vapor phase is relatively low, affecting the selectivity calculation. A similar conclusion arises for the selectivity of R32 over R134a due to the higher amount of R32 in the vapor phase. The

https://doi.org/10.1021/acs.jced.5c00660
J. Chem. Eng. Data 2025, 70, 4939−4953

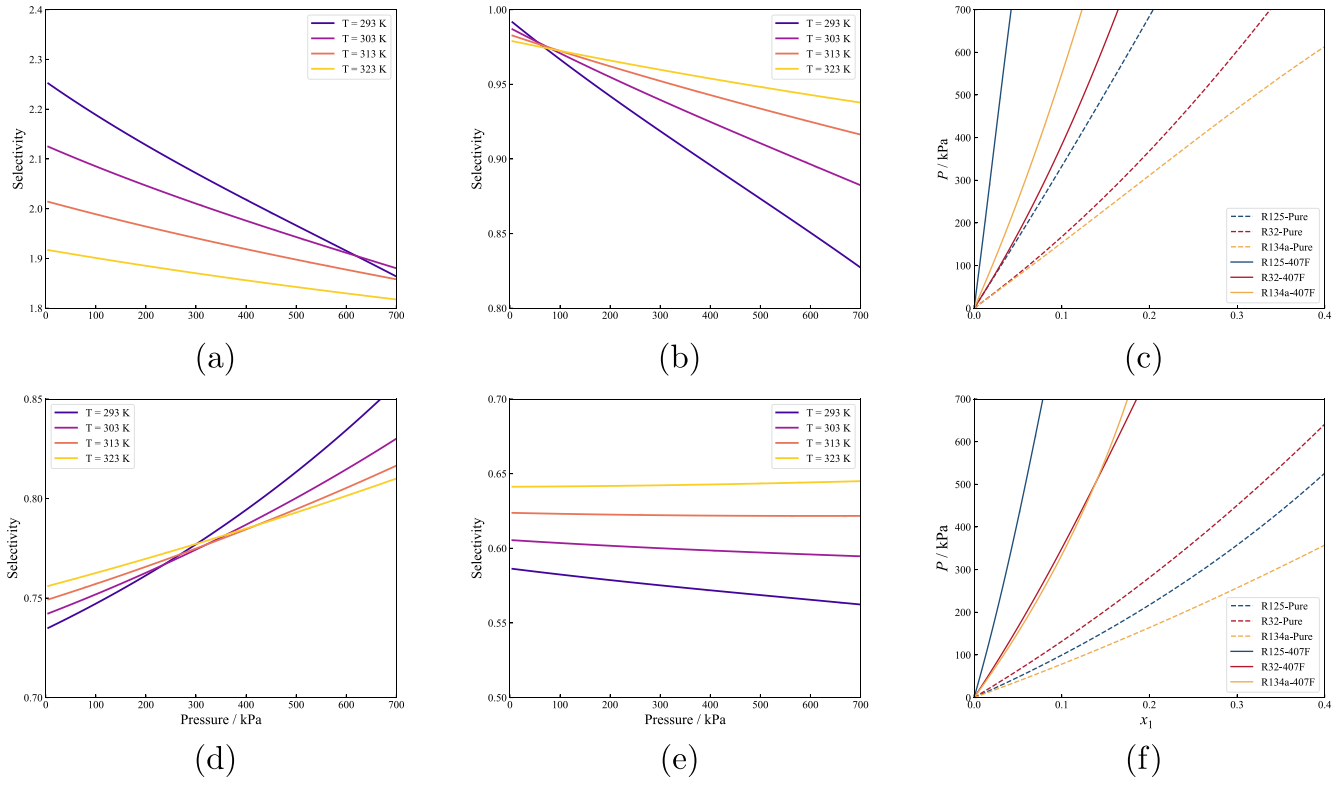

Figure 9. Analysis of the recovery of R32 from the R407F commercial blend. (a) Competitive selectivity of R32 over R125 at different isotherms, (b) competitive selectivity of R32 over R134a at different isotherms, and (c) competitive absorption of R32, R125, and R134a in the R407F blend at 303.15 K in $[C_2mim][CF_3SO_3]$. (d) Competitive selectivity of R32 over R125 at different isotherms, (e) competitive selectivity of R32 over R134a at different isotherms, and (f) competitive absorption of R32, R125, and R134a in the R407F blend at 303.15 K in $[C_2mim][C_4F_9CO_2]$. Dashed lines represent the solubility of the HFCs in the selected ILs when they are being pure.

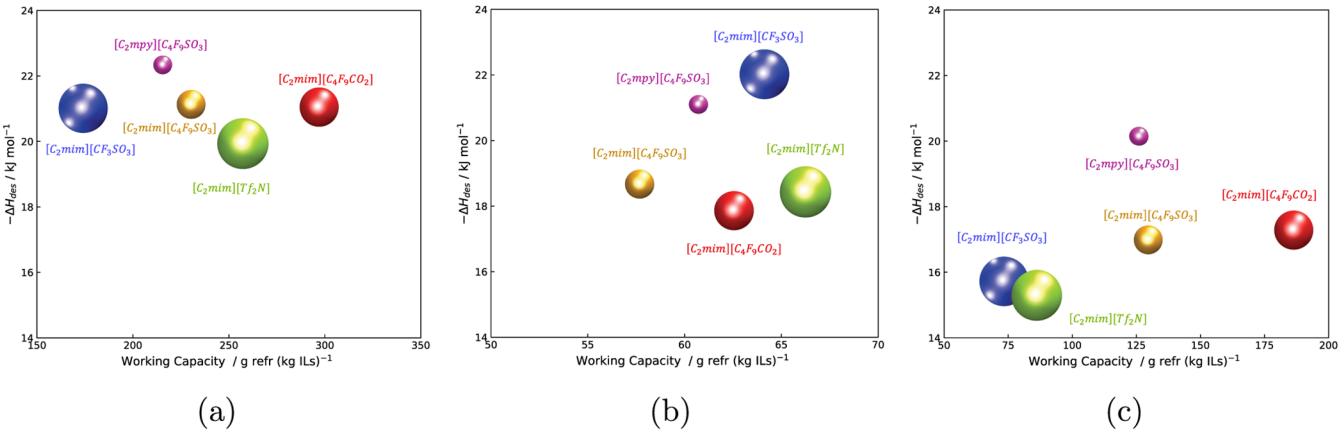

Figure 10. Comparative assessment of the ILs examined in this work for (a) R134a, (b) R32, and (c) R125 absorption. All calculations were obtained from SAFT-VR Mie and the Helmholtz scaling theory using fixed absorption (T_{abs} = 303.15 K, P_{abs} = 500 kPa) and desorption (T_{des} = 343.15 K and P_{abs} = 101.3 kPa) conditions. See the text for details.

performance of the R407F blend in the presence of the remaining ILs is shown in Figure S4.

Key Performance Indicators and Selection of Best Solvents for HFC Recovery. The analysis of the WC and selectivity highlights the delicate balance between these variables and the efficiency of a recovery process based on a commercial blend. In terms of quantity, the working capacity (expressed as grams of refrigerant absorbed per kilogram of solvent) seems to be more reliable for practical applications. However, it is important not to overlook the crucial impact of energy requirements, which are qualitatively represented by the regeneration enthalpy. Finally, the viscosity of the solvent phase also has a strong influence on the mass transfer and pumping requirements. Consequently, these three parameters have been identified as key performance indicators (KPIs) and used to qualitatively assess the best option for recovering the three HFCs studied.

These parameters are graphically plotted in Figure 10 to select the best solvent for R32, R134a, and R125 (note that the separation performance when they are mixed in blends is

https://doi.org/10.1021/acs.jced.5c00660
J. Chem. Eng. Data 2025, 70, 4939−4953

already discussed in the previous subsection). On the one hand, the WC is taken from the results shown in Figure 6b. The enthalpy of regeneration was estimated from the solubility plots for all HFCs and ILs, following the classical thermodynamic relationship:

$$\Delta H_{\mathrm{des}} = R\left(\frac{\partial \ln P_i^{\mathrm{vap}}}{\partial(1/T)}\right)_{x_i} \tag{13}$$

The quantitative numbers are listed in Table 6. Finally, the viscosity of the pure ILs was predicted at the selected absorption conditions (5 bar and 303.15 K) using the Helmholtz scaling theory. These three indicators are plotted together in a combined representation, where round symbols denote the solvents and the marker size is proportional to the solvent viscosity, in a similar manner to that used in other contributions when studying the capacity of ILs to absorb gases.[55] This graphical analysis enables a direct comparison of capacity, energy demand, and process operability across the different systems, providing a holistic screening tool to rank the studied ILs.

Table 6. ΔH_{des} for All of the HFCs and ILs Involved in This Work[a]

ionic liquids	refrigerant	ΔH_{des}, kJ/mol
$[C_2mim][CF_3SO_3]$	R32	−22.038
	R134a	−21.016
	R125	−15.709
$[C_2mim][Tf_2N]$	R32	−18.428
	R134a	−19.931
	R125	−15.289
$[C_2mim][C_4F_9SO_3]$	R32	−18.680
	R134a	−21.128
	R125	−16.981
$[C_2mim][C_4F_9CO_2]$	R32	−17.859
	R134a	−21.041
	R125	−17.287
$[C_2mpy][C_4F_9SO_3]$	R32	−21.099
	R134a	−22.346
	R125	−20.140

[a]Calculations were performed at a constant refrigerant mole fraction x_i = 0.01 (additional calculations at other mole fractions revealed negligible differences in the enthalpy values).

A higher working capacity ensures greater refrigerant recovery per unit solvent, while a lower enthalpy of desorption reduces the thermal energy input required for regeneration. Consequently, the best solvents should be located at the lower right part of the diagram. At the same time, moderate viscosity values are crucial for ensuring efficient handling and minimizing operational costs in large-scale units. As viscosity is inversely proportional to the size of the ball, the higher the volume, the lower the viscosity.

Figure 10a−c show the results for R134a, R32, and R125, respectively. The results for R134a, plotted in Figure 10a, reveal a balance between two possible candidates: the $[C_4F_9CO_2]^-$ anion-based FIL has the highest WC but also a higher viscosity and enthalpy of desorption than the $[Tf_2N]^-$ anion. Hence, both ILs would be the most suitable option among all, with the final choice being dependent on which KPI is prioritized. For the case of R32, in Figure 10b, $[C_2mim][Tf_2N]$ outperforms $[C_2mim][C_4F_9CO_2]$, becoming the best candidate. The situation is quite different for R125, where the low WC of $[C_2mim][Tf_2N]$ makes $[C_2mim][C_4F_9CO_2]$ the best option. Comparing all refrigerants, R134a exhibits the highest values of enthalpy of desorption (in absolute terms), followed by R32 and R125, although the range is relatively narrow (15−23 kJ/mol). These values are in agreement with those found with soft-SAFT by Ferreira et al.[27]

CONCLUSIONS

In this work, the SAFT-VR Mie equation of state was applied for the first time to investigate the thermophysical behavior of the three most common hydrofluorocarbons (HFCs) used in the refrigeration industry, namely, R32, R125, and R134a, in ionic liquids (ILs) with varying degrees of fluorination. Coarse-grained molecular models for these solvents were developed under the ion-pair assumption, specifically assigning a certain number of association sites, and were parametrized using experimental density data, yielding physically consistent parameters with deviations of less than 0.05%. The viscosity of the studied solvents was successfully correlated using the Helmholtz scaling theory in combination with SAFT-VR Mie, providing an accurate quantitative description of their strong temperature dependence.

The solubility of HFCs in these fluorinated ILs was then reproduced using a single, temperature-independent binary interaction parameter (k_{ij}), which remained close to zero for all systems, confirming the transferability and predictive capability of the proposed models. Reliable extrapolations to different temperatures were also tested for $[C_2mim][CF_3SO_3]$ and $[C_2mim][Tf_2N]$, exhibiting good agreement with the experimental data and supporting the model performance for the rest of the ILs under different conditions for process modeling applications.

The working capacity was computed under representative absorption and desorption conditions, providing a quantitative measure of the amount of refrigerant that can be reversibly absorbed. The analysis revealed that the interpretation of working capacity depends strongly on whether it is expressed on a molar or mass basis: while molar quantities are more relevant for thermodynamic analysis, mass-based results are more meaningful for process evaluation and solvent selection. In this context, R134a exhibited the highest absorption capacity across all systems, although the relative performances of R32 and R125 varied notably depending on the chosen basis.

The model was further used to predict competitive selectivities and solubilities for the recovery of refrigerants from multicomponent commercial blends, such as R410A and R407F. The results showed that the vapor-phase fraction in multicomponent mixtures has a strong effect on the calculated selectivity values, an effect that cannot be captured when estimating ideal selectivities from infinite-dilution data. Finally, a set of key performance indicators (KPIs), including working capacity, enthalpy of desorption, and viscosity, was defined to provide a comprehensive assessment of the technical feasibility of each solvent−refrigerant pair, guiding the identification of optimal systems for potential industrial implementation. $[C_2mim][Tf_2N]$ provides the best compromise between energy requirements and overall absorption performance for R32, while $[C_2mim][C_4F_9CO_2]$ stands out as the best option for recovering R125. These two ILs compete as possible candidates for R134a absorption depending on which KPI is prioritized.

https://doi.org/10.1021/acs.jced.5c00660
J. Chem. Eng. Data 2025, 70, 4939−4953

Overall, this study underlines the potential of SAFT-VR Mie, in combination with the Helmholtz scaling theory, as a framework for describing and predicting the thermophysical properties of HFC−IL systems with a good degree of accuracy, becoming a reliable platform to evaluate the behavior of these fluids under different conditions where experimental data are not available.

■ ASSOCIATED CONTENT

Supporting Information

The Supporting Information is available free of charge at https://pubs.acs.org/doi/10.1021/acs.jced.5c00660.

Molecular volume versus molecular weight of the ILs; solubility of R125 in $[C_4F_9SO_3]$ and $[C_2mim][Tf_2N]$; competitive selectivity and solubility of R32 and R125 in the R410A mixture in $[C_2mim][Tf_2N]$, $[C_2mim][C_4F_9SO_3]$, and $[C_2mpy][C_4F_9SO_3]$; and competitive selectivity and solubility of R32, R134a, and R125 in the R407F mixture in $[C_2mim][Tf_2N]$, $[C_2mim][C_4F_9SO_3]$, and $[C_2mpy][C_4F_9SO_3]$. (PDF)

■ AUTHOR INFORMATION

Corresponding Author

Fèlix Llovell − *Department of Chemical Engineering, ETSEQ, Universitat Rovira i Virgili, 43007 Tarragona, Spain;* orcid.org/0000-0001-7109-6810; Email: felix.llovell@urv.cat

Authors

Isaías Huenuvil-Pacheco − *Departamento de Ingeniería Química, Universidad de Concepción, Concepción 4070386, Chile; Department of Chemical Engineering, ETSEQ, Universitat Rovira i Virgili, 43007 Tarragona, Spain;* orcid.org/0009-0006-8381-1141

Andrés Mejía − *Departamento de Ingeniería Química, Universidad de Concepción, Concepción 4070386, Chile;* orcid.org/0000-0001-7238-6633

Complete contact information is available at: https://pubs.acs.org/10.1021/acs.jced.5c00660

Author Contributions

I.H.-P.: methodology, software, formal analysis, writing original draft. A.M.: conceptualization, writing—review and editing, supervision. F.L.: conceptualization, methodology, supervision, project administration, funding acquisition.

Notes

The authors declare no competing financial interest.

■ ACKNOWLEDGMENTS

This research is funded by MICIU/AEI/10.13039/501100011033 through project TED2021-130959B-I00 (European Union NextGenerationEU/PRTR) and project PID2023-149713OB-I00 (ERDF/EU). Additional support from the Chilean National Agency for Research and Development (Agencia Nacional de Investigación y Desarrollo de Chile, ANID) under FONDECYT Project 1230654 is appreciated. Further funding from AGAUR as Consolidated Research Group for AGACAPE (SGR 2021-00738) is gratefully acknowledged. Finally, I.H.-P. thanks the financial support from ANID − Subdirección de Capital Humano, Beca Doctorado Nacional/2022-21222234.

■ REFERENCES

(1) Calm, J. M. The next generation of refrigerants-historical review, considerations, and outlook. *Int. J. Refrig.* **2008**, *31*, 1123−1133.

(2) U.S. Environmental Protection Agency. Overview of Greenhouse Gases: Hydrofluorocarbons 2020 https://www.epa.gov/ghgemissions/overview-greenhouse-gases (accessed September 26, 2025).

(3) Castro, P. J.; Aráujo, J. M. M.; Martinho, G.; Pereiro, A. B. Waste Management Strategies to Mitigate the Effects of Fluorinated Greenhouse Gases on Climate Change. *Appl. Sci.* **2021**, *11*, No. 4367, DOI: 10.3390/app11104367.

(4) Shiflett, M. B.; Yokozeki, A. Separation of refrigerant mixtures using ionic liquids. *Ind. Eng. Chem. Res.* **2010**, *49*, 1370−1377.

(5) Sosa, J. E.; Malheiro, C.; Ribeiro, R. P.; Castro, P. J.; Piñeiro, M. M.; Araújo, J. M.; Plantier, F.; Mota, J. P.; Pereiro, A. B. Adsorption of fluorinated greenhouse gases on activated carbons: evaluation of their potential for gas separation. *J. Chem. Technol. Biotechnol.* **2020**, *95*, 1892−1905.

(6) Akkimaradi, B. S.; Prasad, M.; Dutta, P.; Srinivasan, K. Adsorption of 1,1,1,2-Tetrafluoroethane on Activated Charcoal. *J. Chem. Eng. Data* **2001**, *46*, 417−422.

(7) Ghazy, M.; Harby, K.; Askalany, A. A.; Saha, B. B. Adsorption isotherms and kinetics of activated carbon/Difluoroethane adsorption pair: Theory and experiments. *Int. J. Refrig.* **2016**, *70*, 196−205.

(8) Saha, B. B.; El-Sharkawy, I. I.; Thorpe, R.; Critoph, R. E. Accurate adsorption isotherms of R134a onto activated carbons for cooling and freezing applications. *Int. J. Refrig.* **2012**, *35*, 499−505.

(9) Pardo, F.; Zarca, G.; Urtiaga, A. Separation of Refrigerant Gas Mixtures Containing R32, R134a, and R1234yf through Poly(ether-block-amide) Membranes. *ACS Sustainable Chem. Eng.* **2020**, *8*, 2548−2556.

(10) Shiflett, M. B.; Harmer, M. A.; Junk, C. P.; Yokozeki, A. Solubility and Diffusivity of Difluoromethane in Room-Temperature Ionic Liquids. *J. Chem. Eng. Data* **2006**, *51*, 483−495.

(11) Shiflett, M. B.; Yokozeki, A. Solubility Differences of Halocarbon Isomers in Ionic Liquid [emim][Tf2N]. *J. Chem. Eng. Data* **2007**, *52*, 2007−2015.

(12) Ren, W.; Scurto, A. M. Phase Equilibria of Imidazolium Ionic Liquids and the Refrigerant Gas, 1,1,1,2-Tetrafluoroethane (R-134a). *Fluid Phase Equilib.* **2009**, *286*, 1−7.

(13) Dong, L.; Zheng, D.; Sun, G.; Wu, X. Vapor-Liquid Equilibrium Measurements of Difluoromethane + [Emim]OTf, Difluoromethane + [Bmim]OTf, Difluoroethane + [Emim]OTf, and Difluoroethane + [Bmim]OTf Systems. *J. Chem. Eng. Data* **2011**, *56*, 3663−3668.

(14) Sosa, J. E.; Ribeiro, R. P. P. L.; Castro, P. J.; Mota, J. P. B.; Araújo, J. M. M.; Pereiro, A. B. Absorption of Fluorinated Greenhouse Gases Using Fluorinated Ionic Liquids. *Ind. Eng. Chem. Res.* **2019**, *58*, 20769−20778.

(15) Castro, P. J.; Redondo, A. E.; Sosa, J. E.; Zakrzewska, M. E.; Nunes, A. V. M.; Araújo, J. M. M.; Pereiro, A. B. Absorption of Fluorinated Greenhouse Gases in Deep Eutectic Solvents. *Ind. Eng. Chem. Res.* **2020**, *59*, 13246−13259.

(16) Ferreira, M. L.; Pastoriza-Gallego, M. J.; Araújo, J. M. M.; Canongia Lopes, J. N.; Rebelo, L. P. N.; Piñeiro, M. M.; Shimizu, K.; Pereiro, A. B. Influence of Nanosegregation on the Phase Behavior of Fluorinated Ionic Liquids. *J. Phys. Chem. C* **2017**, *121*, 5415−5427.

(17) Hu, Y.-F.; Liu, Z.-C.; Xu, C.-M.; Zhang, X.-M. The molecular characteristics dominating the solubility of gases in ionic liquids. *Chem. Soc. Rev.* **2011**, *40*, 3802−3823.

(18) Pereiro, A. B.; Tomé, L. C.; Martinho, S.; Rebelo, L. P. N.; Marrucho, I. M. Gas Permeation Properties of Fluorinated Ionic Liquids. *Ind. Eng. Chem. Res.* **2013**, *52*, 4994−5001.

(19) Pereiro, A. B.; Araújo, J. M. M.; Martinho, S.; Alves, F.; Nunes, S.; Matias, A.; Duarte, C. M. M.; Rebelo, L. P. N.; Marrucho, I. M. Fluorinated Ionic Liquids: Properties and Applications. *ACS Sustainable Chem. Eng.* **2013**, *1*, 427−439.

(20) Vieira, N. S.; Ferreira, M. L.; Castro, P. J.; Araújo, J. M.; Pereiro, A. B. *Ionic Liquids - Thermophysical Properties and*

Applications; Murshed, S. M. S., Ed.; IntechOpen: London, 2021, Chapter 2.
(21) Kim, Y. J.; Kim, S.; Joshi, Y. K.; Fedorov, A. G.; Kohl, P. A. Thermodynamic analysis of an absorption refrigeration system with ionic-liquid/refrigerant mixture as a working fluid. *Energy* **2012**, *44*, 1005−1016.
(22) Baca, K. R.; Al-Barghouti, K.; Wang, N.; Bennett, M. G.; Matamoros Valenciano, L.; May, T. L.; Xu, I. V.; Cordry, M.; Haggard, D. M.; Haas, A. G.; et al. Ionic liquids for the separation of fluorocarbon refrigerant mixtures. *Chem. Rev.* **2024**, *124*, 5167−5226.
(23) Sosa, J. E.; Santiago, R.; Hospital-Benito, D.; Costa Gomes, M.; Araújo, J. M. M.; Pereiro, A. B.; Palomar, J. Process Evaluation of Fluorinated Ionic Liquids as F-Gas Absorbents. *Environ. Sci. Technol.* **2020**, *54*, 12784−12794. PMID: 32822151.
(24) Sosa, J. E.; Santiago, R.; Redondo, A. E.; Avila, J.; Lepre, L. F.; Gomes, M. C.; Araújo, J. M. M.; Palomar, J.; Pereiro, A. B. Design of Ionic Liquids for Fluorinated Gas Absorption: COSMO-RS Selection and Solubility Experiments. *Environ. Sci. Technol.* **2022**, *56*, 5898−5909. PMID: 35435682.
(25) Blas, F. J.; Vega, L. F. Thermodynamic behaviour of homonuclear and heteronuclear Lennard-Jones chains with association sites from simulation and theory. *Mol. Phys.* **1997**, *92*, 135−150.
(26) Jovell, D.; Gómez, S. B.; Zakrzewska, M. E.; Nunes, A. V. M.; Araújo, J. M. M.; Pereiro, A. B.; Llovell, F. Insight on the Solubility of R134a in Fluorinated Ionic Liquids and Deep Eutectic Solvents. *J. Chem. Eng. Data* **2020**, *65*, 4956−4969.
(27) Ferreira, M. L.; Araújo, J. M. M.; Vega, L. F.; Pereiro, A. B. Understanding the Absorption of Fluorinated Gases in Fluorinated Ionic Liquids for Recovering Purposes Using Soft-SAFT. *J. Chem. Eng. Data* **2022**, *67*, 1951−1963.
(28) Demirbek, M. G.; Rodriguez Reartes, S. B.; Llovell, F. Thermodynamic Analysis of the Absorption of Common Refrigerants in Fluorinated Deep Eutectic Solvents. *Fluid Phase Equilib.* **2024**, *581*, 114077.
(29) Alencar, L.; González-Barramuño, B.; Rodriguez-Reartes, S.; Quinteros-Lama, H.; Garrido, J.; Codera, V.; Pou, J.; Tavares, F.; Gonzalez-Olmos, R.; Llovell, F. Thermophysical Characterization of Sustainable Pathways for Hydrofluorocarbons Separation Utilizing Deep Eutectic Solvents. *J. Ind. Eng. Chem.* **2025**, *146*, 788−799.
(30) Lafitte, T.; Apostolakou, A.; Avendaño, C.; Galindo, A.; Adjiman, C. S.; Müller, E. A.; Jackson, G. Accurate statistical associating fluid theory for chain molecules formed from Mie segments. *J. Chem. Phys.* **2013**, *139*, No. 154504, DOI: 10.1063/1.4819786.
(31) Paricaud, P. Multipolar SAFT-VR Mie equation of state: Predictions of phase equilibria in refrigerant systems with no binary interaction parameter. *J. Phys. Chem. B* **2023**, *127*, 3052−3070.
(32) Chiko, A.; Polishuk, I.; Cea-Klapp, E.; Garrido, J. M. Comparison of CP-PC-SAFT and SAFT-VR-Mie in Predicting Phase Equilibria of Binary Systems Comprising Gases and 1-Alkyl-3-methylimidazolium Ionic Liquids. *Molecules* **2021**, *26*, No. 6621, DOI: 10.3390/molecules26216621.
(33) Chapman, W. G.; Gubbins, K. E.; Jackson, G.; Radosz, M. New reference equation of state for associating liquids. *Ind. Eng. Chem. Res.* **1990**, *29*, 1709−1721.
(34) Dufal, S.; Lafitte, T.; Haslam, A. J.; Galindo, A.; Clark, G. N.; Vega, C.; G, J. The A in SAFT: developing the contribution of association to the Helmholtz free energy within a Wertheim TPT1 treatment of generic Mie fluids. *Mol. Phys.* **2015**, *113*, 948−984.
(35) Gross, J.; Vrabec, J. An equation-of-state contribution for polar components: dipolar molecules. *AIChE J.* **2006**, *52*, 1194−1204.
(36) Huang, S. H.; Radosz, M. Equation of State for Small, Large, Polydisperse, and Associating Molecules. *Ind. Eng. Chem. Res.* **1990**, *29*, 2284−2294.
(37) Tan, S. P.; Adidharma, H.; Radosz, M. Generalized procedure for estimating the fractions of nonbonded associating molecules and their derivatives in thermodynamic perturbation theory. *Ind. Eng. Chem. Res.* **2004**, *43*, 203−208.
(38) Mejía, A.; Müller, E. A.; Chaparro Maldonado, G. SGTPy: A Python code for calculating the interfacial properties of fluids based on the square gradient theory using the SAFT-VR Mie equation of state. *J. Chem. Inf. Model.* **2021**, *61*, 1244−1250.
(39) Gonçalves, C. I. S.; Silva, G. M.; Ndiaye, P. M.; Tavares, F. W. Helmholtz scaling: an alternative approach to calculate viscosity with the PCP-saft equation of state. *Ind. Eng. Chem. Res.* **2021**, *60*, 9231−9245.
(40) Huenuvil-Pacheco, I.; Cartes, M.; Mejía, A. Toward sustainable fuel formulations: thermophysical assessment of a synthetic oxygenated blend formed from hexane+ cyclopentyl methyl ether+ propan-1-ol. *Sustainable Energy Fuels* **2025**, *9*, 4959−4973.
(41) Neufeld, P. D.; Janzen, A.; Aziz, R. Empirical equations to calculate 16 of the transport collision integrals Ω (l, s)* for the Lennard-Jones (12−6) potential. *J. Chem. Phys.* **1972**, *57*, 1100−1102.
(42) Urahata, S. M.; Ribeiro, M. C. C. Single particle dynamics in ionic liquids of 1-alkyl-3-methylimidazolium cations. *J. Chem. Phys.* **2005**, *122*, 024511.
(43) Ferreira, M. L.; Araújo, J. M. M.; Pereiro, A. B.; Vega, L. F. Insights into the influence of the molecular structures of fluorinated ionic liquids on their thermophysical properties. A soft-SAFT based approach. *Phys. Chem. Chem. Phys.* **2019**, *21*, 6362−6380.
(44) Huenuvil-Pacheco, I.; Viar, M.; Zarca, G.; Urtiaga, A.; Mejía, A.; Llovell, F. Manuscript submitted to Energy (Manuscript No. EGY-D-25-19364).
(45) Sequeira, M. C.; Avelino, H. M.; Caetano, F. J.; Fareleira, J. M. Viscosity measurements of 1-ethyl-3-methylimidazolium trifluoromethanesulfonate (EMIM OTf) at high pressures using the vibrating wire technique. *Fluid Phase Equilib.* **2020**, *505*, 112354.
(46) Gardas, R. L.; Freire, M. G.; Carvalho, P. J.; Marrucho, I. M.; Fonseca, I. M.; Ferreira, A. G.; Coutinho, J. A. P ρ T measurements of imidazolium-based ionic liquids. *J. Chem. Eng. Data* **2007**, *52*, 1881−1888.
(47) Vieira, N. S. M.; Reis, P. M.; Shimizu, K.; Cortes, O. A.; Marrucho, I. M.; Araújo, J. M. M.; Esperança, J. M. S. S.; Lopes, J. N. C.; Pereiro, A. B.; Rebelo, L. P. N. A thermophysical and structural characterization of ionic liquids with alkyl and perfluoroalkyl side chains. *RSC Adv.* **2015**, *5*, 65337−65350.
(48) Vieira, N.; Luís, A.; Reis, P.; Carvalho, P.; Lopes-da Silva, J.; Esperança, J.; Araújo, J.; Rebelo, L.; Freire, M.; Pereiro, A. Fluorination effects on the thermodynamic, thermophysical and surface properties of ionic liquids. *J. Chem. Thermodyn.* **2016**, *97*, 354−361.
(49) Albà, C. G.; Alkhatib, I. I. I.; Llovell, F.; Vega, L. F. Assessment of Low Global Warming Potential Refrigerants for Drop-In Replacement by Connecting their Molecular Features to Their Performance. *ACS Sustainable Chem. Eng.* **2021**, *9*, 17034−17048.
(50) Liu, Q.; Ma, L.; Wang, S.; Ni, Z.; Fu, X.; Wang, J.; Zheng, Q. Study on the properties of density, viscosity, excess molar volume, and viscosity deviation of [C2mim][NTf2], [C2mmim][NTf2], [C4mim][NTf2], and [C4mmim][NTf2] with PC binary mixtures. *J. Mol. Liq.* **2021**, *325*, 114573.
(51) Asensio-Delgado, S.; Pardo, F.; Zarca, G.; Urtiaga, A. Vapor-Liquid Equilibria and Diffusion Coefficients of Difluoromethane, 1,1,1,2-Tetrafluoroethane, and 2,3,3,3-Tetrafluoropropene in Low-Viscosity Ionic Liquids. *J. Chem. Eng. Data* **2020**, *65*, 4242−4251.
(52) Han, X.; Chen, G.; Cui, X.; Wang, Q. Vapor- liquid equilibrium data for the binary mixture difluoroethane (HFC-32)+ pentafluoroethane (HFC-125) of an alternative refrigerant. *J. Chem. Eng. Data* **2007**, *52*, 2112−2116.
(53) Kato, R.; Nishiumi, H. Vapor-liquid equilibria and critical loci of binary and ternary systems composed of CH2F2, C2HF5 and C2H2F4. *Fluid Phase Equilib.* **2006**, *249*, 140−146.
(54) Lee, B. G.; Park, J. Y.; Lim, J. S.; Cho, S. Y.; Park, K. Y. Phase equilibria of chlorofluorocarbon alternative refrigerant mixtures. *J. Chem. Eng. Data* **1999**, *44*, 190−192.
(55) Alkhatib, I. I. I.; Ferreira, M. L.; Alba, C. G.; Bahamon, D.; Llovell, F.; Pereiro, A. B.; Araújo, J. M. M.; Abu-Zahra, M. R.; Vega, L. F. Screening of Ionic Liquids and Deep Eutectic Solvents for Physical

CO2 Absorption by Soft-SAFT Using Key Performance Indicators. *J. Chem. Eng. Data* **2020**, *65*, 5844−5861.

https://doi.org/10.1021/acs.jced.5c00660
J. Chem. Eng. Data 2025, 70, 4939−4953